Available online at www.sciencedirect.com

SciVerse ScienceDirect

Ceramics International 39 (2013) 5235–5239

CERAMICS INTERNATIONAL

www.elsevier.com/locate/ceramint

Structural and magnetic properties of ZnMg-ferrite nanoparticles prepared using the co-precipitation method

S. Rahman[a], K. Nadeem[a,*], M. Anis-ur-Rehman[b], M. Mumtaz[a], S. Naeem[a], I. Letofsky-Papst[c]

[a]*Materials Research Laboratory, Department of Physics, International Islamic University, Islamabad, Pakistan*
[b]*Applied Thermal Physics Laboratory, Department of Physics, COMSATS Institute of Information Technology, Islamabad, Pakistan*
[c]*Institute for Electron Microscopy, University of Technology Graz, Steyrergasse 17, A-8010 Graz, Austria*

Received 12 November 2012; received in revised form 7 December 2012; accepted 8 December 2012
Available online 20 December 2012

Abstract

We synthesized soft magnetic spinel ferrite ZnMg-ferrite ($Zn_{1-x}Mg_xFe_2O_4$, where $x=0.0$, 0.1, 0.2, 0.3, 0.4, and 0.5) nanoparticles using the co-precipitation method. Structural and magnetic properties have been studied in detail. XRD revealed that the structure of these nanoparticles is spinel with crystallite size lies in the range 21–31 nm. Lattice parameter decreases with increasing Mg concentration due to the smaller ionic radius of the Mg^{2+} ion. FTIR spectroscopy also confirmed the formation of spinel ferrite by showing the characteristic absorption bands at 420 cm^{-1} and 545 cm^{-1}. Vibrational band of metal ion at tetrahedral site ($M_{tet.}$) with oxygen ions (O–$M_{tet.}$–O) is shifted toward higher wave numbers with the increase of Mg concentration. The magnetization showed an increasing trend with increasing Mg concentration due to the rearrangement of cations at tetrahedral and octahedral sites, while the corecivity remained constant due to the soft nature of the ferrite composition. Both structural and magnetic properties of ZnMg-ferrite nanoparticles strongly depend upon Mg^{2+} cation doping percentage.

Keywords: D. Ferrites; Spinel structure; Nanoparticles

1. Introduction

Mixed spinel ferrites have been studied intensively over the last few years due to their potential applications [1–3]. Spinel ferrites have the chemical formula MFe_2O_4 in which M can be any divalent metal cation. In spinel ferrite, oxygen forms an FCC-lattice with divalent cations at tetrahedral (A) and/or octahedral (B) sites. The unit cell of a spinel ferrite consists of 32 oxygen, 16 trivalent iron and 8 divalent metal ions [4]. The spins at tetrahedral and octahedral lattice sites are anti-parallel to each other. Preference of divalent metal ion M^{2+} depends upon the type of the spinel structure e.g. normal, inverse and mixed spinel structures. In case of inverse spinel structure, e.g. nickel ferrite and cobalt ferrite, Fe^{3+} ions are distributed equally over both lattice sites and divalent metal M^{2+} ions that prefer B sites. Physical properties are strongly influenced by the preference of metal ions on these lattice sites [5]. The structural and magnetic environments of these two lattice sites can be controlled by the chemical composition, synthesis methods, and annealing temperature. The concentration and types of cations substitution also have very dominant effects on the physical properties [6,7]. Magnesium ferrite ($MgFe_2O_4$) has an inverse spinel structure with the preference of Mg^{2+} cations mainly on octahedral sites [8–10], while zinc ferrite ($ZnFe_2O_4$) has normal spinel structure, in which Zn^{2+} cations mainly occupy tetrahedral sites [11,12]. Both Zn^{2+} and Mg^{2+} divalent ions are non-magnetic in nature. In this article, we will focus on the influence of magnesium divalent caions doping on structural and magnetic properties of zinc ferrite nanoparticles.

*Corresponding author. Tel.: +92 519019714.
E-mail address: kashif.nadeem@iiu.edu.pk (K. Nadeem).

0272-8842/$ - see front matter © 2012 Elsevier Ltd and Techna Group S.r.l. All rights reserved.
http://dx.doi.org/10.1016/j.ceramint.2012.12.023

2. Experiment

ZnMg-ferrite ($Zn_{1-x}Mg_xFe_2O_4$) nanoparticles with composition $x=0.0$, 0.1, 0.2, 0.3, 0.4, and 0.5 were synthesized using a conventional co-precipitation method. The chemical co-precipitation technique is comparatively easy to scale up and widely used to synthesize ferrite nanoparticles. The chemical reagents used in this experiment were ferric nitrate $Fe(NO_3)_3\cdot 9H_2O$, zinc nitrate $Zn(NO_3)_2\cdot 6H_2O$ and magnesium nitrate $Mg(NO_3)_2\cdot 6H_2O$. All the chemical reagents were of analytical grade and used without any purification.

Solutions of $Zn(NO_3)_2\cdot 6H_2O$, $Mg(NO_3)_2\cdot 6H_2O$ and $Fe(NO_3)_3\cdot 9H_2O$ in their stoichiometry were dissolved in distilled water under constant stirring, until a clear solution was obtained. To obtain ferrite nanoparticles which are less dispersed in size, of smaller size and more chemically homogeneous, the mixing of reagents was carried out very quickly by adding the precipitating reagent NaOH rapidly into metal solutions at constant stirring till co-precipitation occurred. The solution was kept at temperature of 70 °C for 45 min for transformation of the hydroxides into ferrites. The pH value was maintained in the range of 12–13. Distilled water was used to clean precipitates until these precipitates were free from chloride and sodium ions. Washed precipitates were dried in an oven at temperature 100 °C for 12 h to remove water content. At the end, dried powder was mixed homogeneously in mortar and agate for 25 min to get the desired ZnMg-ferrite nanopartticles.

All synthesis parameters were kept constant except for the concentration of divalent cations (Mg^{2+} and Zn^{2+}). Structural characterization was done using X-ray diffraction (XRD), Fourier transform infrared (FTIR) spectroscopy and transmission electron microscopy (TEM). Magnetic characterization was done using a vibrating sample magnetometer (VSM).

3. Results and discussion

X-ray diffraction (XRD) was carried out using Cu-K_α (0.154 nm) radiation at ambient temperature. Fig. 1 shows the X-ray diffraction patterns of samples $Zn_{1-x}Mg_xFe_2O_4$ nanoparticles with x in the range 0.0–0.5. All the indexed peaks correspond to spinel ferrite structure for all the samples and therefore confirm the formation of spinel ferrite nanoparticles. Average crystallite sizes using all indexed peaks for each sample were estimated by using the Debye–Scherrer's formula and is in the range 21–31 nm for different Mg concentrations.

The average crystallite size was calculated (for all the indexed peaks) using the Debye–Scherrer's formula as given in Eq. (1):

$$t = 0.9\lambda/\beta\cos\theta \quad (1)$$

where t is the average crystallite size, θ is the diffraction angle, λ is the wavelength of incident X-ray and β is the full width half maximum of the XRD peak in units of radians.

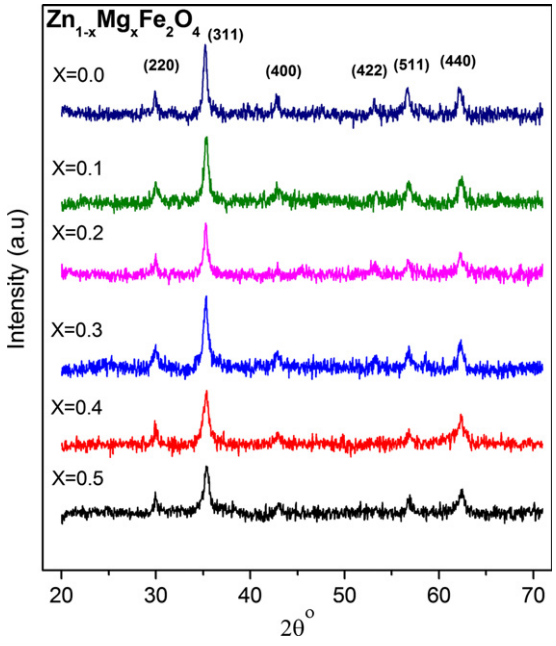

Fig. 1. XRD patterns of $Zn_{1-x}Mg_xFe_2O_4$ nanoparticles with x in the range 0.0–0.5.

The average crystallite size vs. Mg concentration is plotted in Fig. 2(a). Average crystallite size scatters in the range 21–31 nm for different compositions. It has a minimum crystallite size 21 nm for $x=0.5$ Mg concentration due to the smaller ionic radius of Mg^{2+} ions.

The lattice parameter 'a' was estimated using lattice spacing (d) values and respective miller indices ($h\,k\,l$). The lattice constant 'a' was calculated by using the formula as given in Eq. (2):

$$a = d/\sqrt{h^2+k^2+l^2} \quad (2)$$

where a is the lattice parameter, d is the lattice spacing and h, k, l are the miller indices. The lattice parameter obtained by using XRD data lies in the range of 8.40–8.43 Å for different Mg concentrations as shown in Fig. 2(b). It decreases with increasing Mg concentration due to the smaller ionic radius of Mg^{2+} (0.06 nm) cation as compared to ionic radius of Zn^{2+} (0.08 nm) cation [13,14].

Transmission electron microscopy (TEM) micrograph of one of the samples with composition $Zn_{0.8}Mg_{0.2}Fe_2O_4$ at 100 nm scale is shown in Fig. 3. TEM image reveals that the nanoparticles are nearly spherical in shape and have narrow particle size distribution. Nanoparticles are agglomerated due to the presence of magnetic interactions among particles.

Vibronic studies using infrared radiation are a good fingerprint for the local chemical bonds [15]. Formation of ferrite nanoparticles has been also studied by FTIR spectroscopy in the far-infrared region 400–660 cm^{-1} as shown in Fig. 4. FTIR absorption measurements were carried out using the KBr pellet technique. In spinel ferrites, the bands in the ranges of 545–575 cm^{-1} and 420–430 cm^{-1} are usually assigned to tetrahedral and

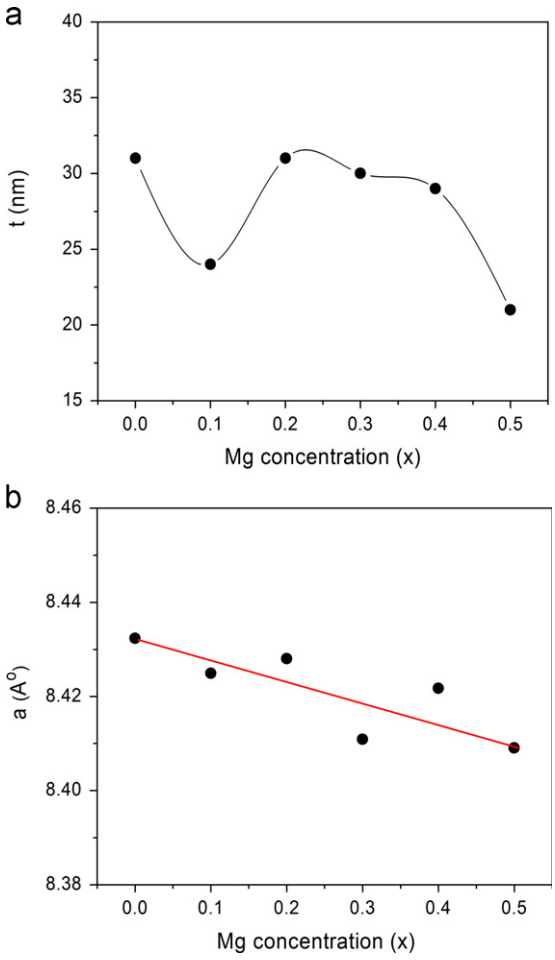

Fig. 2. (a) Plot of average crystallite size 't' vs. Mg concentration, and (b) plot of lattice constant 'a' vs. Mg concentration of $Zn_{1-x}Mg_xFe_2O_4$ nanoparticles with x in the range 0.0–0.5. Solid lines just show the trend.

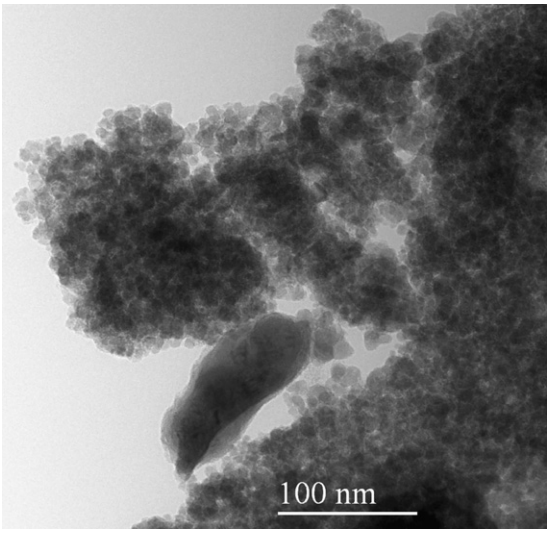

Fig. 3. TEM micrograph of $Zn_{0.8}Mg_{0.2}Fe_2O_4$ nanoparticles at 100 nm scale.

octahedral ions vibrations with oxygen ions, respectively, which are also characteristic bands of spinel ferrite. The band at 420 cm^{-1} is due to the vibration of the chemical

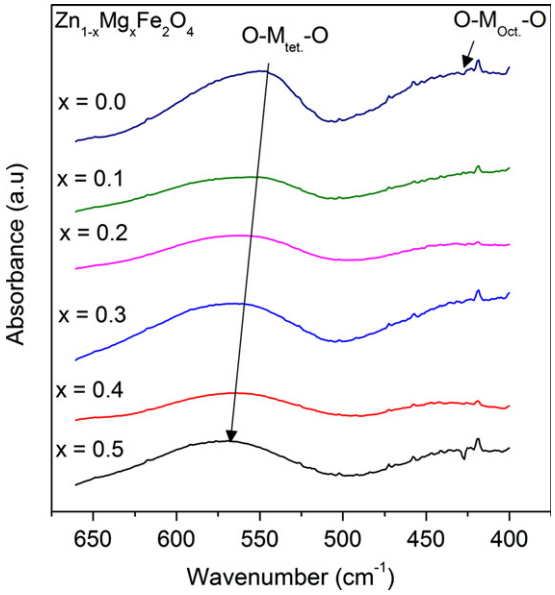

Fig. 4. Far-infrared spectra of KBr-pelletized nanoparticles samples $Zn_{1-x}Mg_xFe_2O_4$ with x in the range 0.0–0.5. Bands at 545 and 420 cm^{-1} correspond to tetrahedral and octahedral site coordination of metal ions with oxygen in the spinel crystal structure, respectively. Arrow indicates the shift of $O–M_{tet.}–O$ vibration band with increasing Mg concentration.

bond $O–M_{Oct.}–O$ in location of octahedron and the band at 545 cm^{-1} is due to the vibration of the chemical bond $O–M_{tet.}–O$ in location of tetrahedron. The presence of these absorption bands signifies the formation of spinel structure of zinc ferrite. It is also observed that the $O–M_{tet.}–O$ band is shifted to higher wave numbers with the increase in Mg concentration (as indicated by an arrow in Fig. 4). Keny et al. [16] reported a shift of a tetrahedral band of Mg ferrite toward higher wave number as compared to the Zn ferrite. The shift of the $O–M_{tet.}–O$ vibration band with increasing Mg concentration signifies the preference of Mg ions in tetrahedral lattice sites in addition to octahedral sites. Pradeep et al. [8] reported that the Mg^{2+} ions prefer both tetrahedral and octahedral sites in Mg ferrite nanoparticles.

Magnetization measurements were carried out using a vibrating sample magnetometer (VSM) at room temperature with a maximum applied magnetic field of 8 kOe. Fig. 5(a) shows the MH-loop of pure Zn ferrite nanoparticles at room temperature. Magnetization of mixed spinel ferrites nanoparticles is strongly influenced by the cationic distribution on tetrahedral and octahedral lattice sites. Pure zinc ferrite ($x=0.0$) nanoparticles show a paramagnetic like loop with hysteresis (due to surface effects in ferrite nanoparticles) due to its normal spinel structure. Bulk zinc ferrite exhibits normal spinel structure in which Zn^{2+} and Fe^{3+} ions are distributed on tetrahedral and octahedral sites, respectively. The presence of hysteresis in zinc ferrite nanoparticles (see the inset of Fig. 5(a)) is due to incomplete normal or mixed spinel structure of zinc ferrite nanoparticles and/or due to the presence of disordered surface spins [17–19].

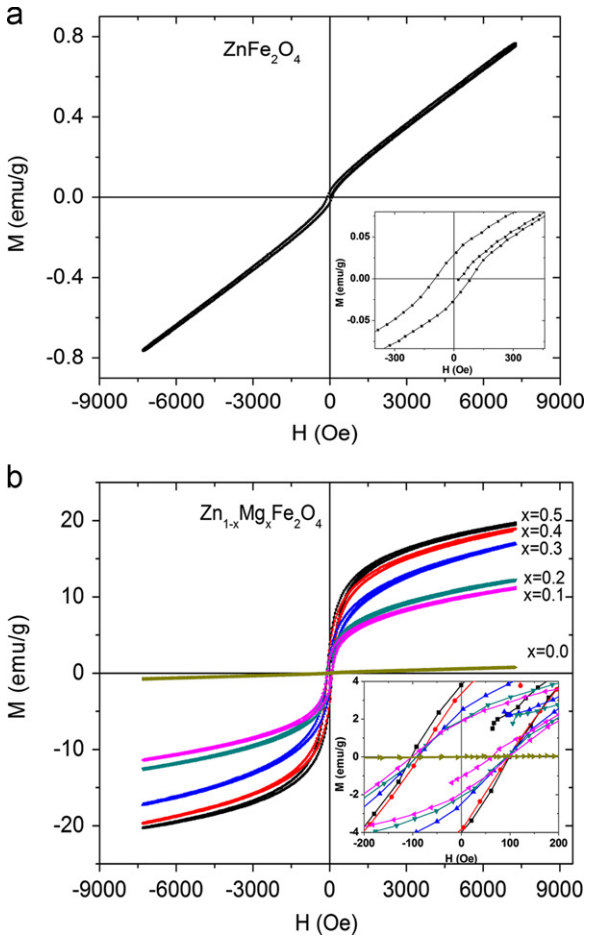

Fig. 5. (a) MH-loop of pure zinc ferrite ($ZnFe_2O_4$) nanoparticles sample, and (b) MH-loops of the samples $Zn_{1-x}Mg_xFe_2O_4$ with x in the range 0.0–0.5. Insets in both figures show the coercivity region.

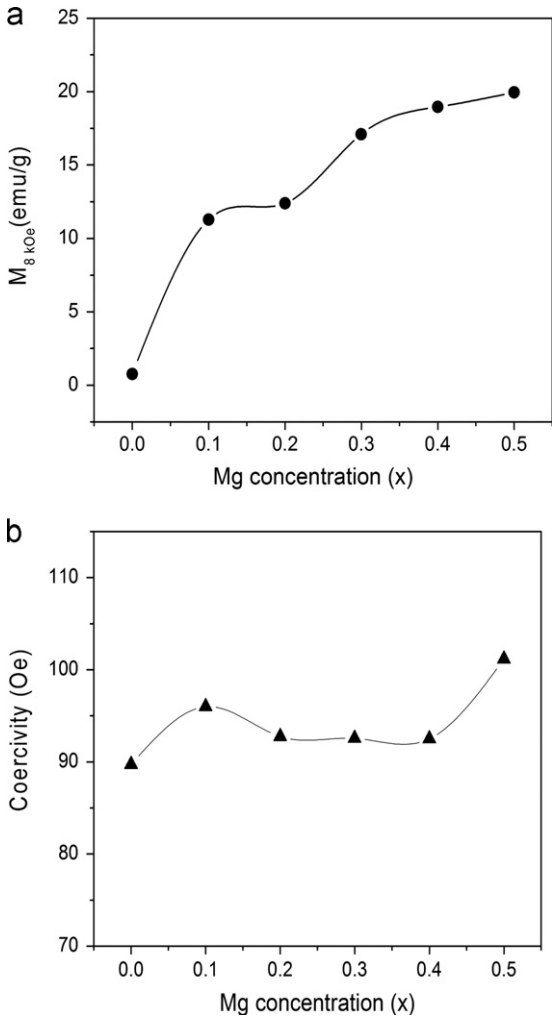

Fig. 6. (a) Variation of the magnetization at 8 kOe ($M_{8\ kOe}$) vs. Mg concentration, and (b) variation of the coercivity (H_c) vs. Mg concentration.

Magnetization parameters such as coercivity (H_c) and magnetization at 8 kOe ($M_{8\ kOe}$) were calculated from Fig. 5(b) and are shown in Fig. 6(a,b). The magnetization at maximum field of 8 kOe monotonically increases with increasing Mg concentration as illustrated in Fig. 6(a). In spinel ferrites, magnetic moments at tetrahedral and octahedral lattice sites are anti-parallel to each other [20]. In the literature, it is reported that the pure bulk Mg ferrite exhibits inverse spinel structure in which Mg^{2+} ions prefer octahedral sites, while in nanoparticles form Mg ferrite shows magnetic behavior due to its incomplete inverse spinel structure at nano-scale [8–10]. Increase of the net magnetization with increasing Mg concentration is due to the misbalance of Fe^{3+} ions on octahedral and tetrahedral lattice sites. Misbalance of Fe^{3+} ions strengthens the A–B superexchange interactions which results in the increase of the net magnetization [21]. Therefore the magnetization of ZnMg-ferrite nanoparticles depends on the distribution of Fe^{3+} ions among tetrahedral and octahedral lattices sites because both Mg^{2+} and Zn^{2+} ions are non-magnetic in nature. In nanoparticles, spins on the surface of nanoparticles also play an important role in determining magnetic properties [22,23]. It can affect the overall magnetic behavior of individual nanoparticles [24,25]. The decrease of magnetization with decreasing diameter of ferrite nanoparticles is a very well known effect, since the surface to volume ratio becomes of significant importance. The atoms on the surface have truncated bonds and less coordination neighbors, thus their mutual exchange interaction is reduced due to surface disorders. This surface disorder is due to bond frustration of exchange interaction between ferrimagnetically coupled spins of different sublattices near the surface [26]. As the particle size gets smaller, such disorder and frustration at the nanoparticle's surface become progressively dominant due to large surface to volume ratio. Kodama and Berkowitz [27] reported a model for magnetization (M) of fine nanoparticles which shows a decrease in M with diminishing particle size due to the presence of disordered surface spins. In our case, although sample with $x=0.5$ Mg concentration has minimum crystallite size (21 nm) we still got the maximum magnetization for it, which indicates the dominance of cationic distribution over size effects in our

samples. The coercivity (H_c) fluctuates in the range of 90–100 Oe as the Mg concentration is increased from 0.0 to 0.5. Smaller values of coercivity for all the samples indicate the soft magnetic nature of these ferrite nanoparticles and also the presence of ferrimagnetic behavior at room temperature.

4. Conclusions

Zinc ferrite nanoparticles doped with Mg cations ($Zn_{1-x}Mg_xFe_2O_4$ with x in the range 0.0–0.5) were sucessfully synthesized by the co-precipitation method. Initial structural characterization was done by using X-ray diffraction analysis. Average crystallite size was calculated by Debye Scherrer's formula which lies in the range of 21–31 nm for different compositions. The lattice parameter decreases with increasing Mg concentration due to the smaller ionic radius of Mg^{2+} ion as compared to the Zn^{2+} ion. TEM images show that there is not so much scattering in the particle size and nanoparticles are nearly spherical in shape. Specific vibrational bands in FTIR spectroscopy signify the formation of spinel Zn-Mg ferrite nanoparticles which is in agreement with the XRD data. FTIR results revealed the shift of vibration band located at tetrahedral site with increasing Mg concentration which is due to changes in the local chemical environment and bond lengths. On doping Mg cations, ferromagnetic behavior increases which changes the shape of MH-loops. The magnetization at the maximum field monotonically increases with increasing Mg concentration which is attributed to the change in the cationic distribution at tetrahedral and octahedral sites. Smaller values of the coercivity show the soft magnetic nature of these ZnMg-ferrite nanoparticles.

It can be concluded that different changes occur in the properties of Mg doped Zn-ferrite nanoparticles due to the rearrangements of divalent metal cations at different lattice sites.

Acknowledgments

The authors acknowledge Higher Education Commission (HEC) of Pakistan for providing research funds.

References

[1] M. Srivastava, A.K. Ojha, S. Chaubey, A. Materny, Journal of Alloys and Compounds 481 (2009) 515.
[2] L. Yang, Y. Xie, H. Zhao, X. Wu, Y. Wang, Solid-State Electronics 49 (2005) 1029.
[3] E. Hee Kim, H. Sook Lee, B. Kook Kwak, B. Kim, Journal of Magnetism and Magnetic Materials 289 (2005) 328.
[4] J. Smit, H.P.J. Wijn, Ferrites—Physical Properties of Ferromagnetic Oxides in Relation to Their Technical Applications, Wiley, New York, 1959.
[5] E. Rezlescu, E.L. Sachelarie, N. Rezlescu, Journal of Optoelectronics and Advanced Materials 8 (2006) 1019–1022.
[6] A.M. Abdeen, Journal of Magnetism and Magnetic Materials 185 (1998) 199.
[7] M.A. El Hiti, Journal of Magnetism and Magnetic Materials 192 (1999) 305.
[8] A. Pradeep, P. Priyadharsini, G. Chandrasekaran, Journal of Magnetism and Magnetic Materials 320 (2008) 2774.
[9] V. Šepelak, D. Baabe, D. Mienert, F.J. Litterst, K.D. Becker, Scripta Materialia 48 (2003) 961.
[10] Y. Ichiyanagi, M. Kubota, S. Moritake, Y. Kanazawa, T. Yamada, T. Uehashi, Journal of Magnetism and Magnetic Materials 310 (2007) 2378.
[11] K.P. Thummer, M.C. Chhantbar, K.B. Modi, G.J. Baldha, H.H. Joshi, Journal of Magnetism and Magnetic Materials 280 (2004) 23–30.
[12] R.G. Kulkarni, H.H. Joshi, Solid State Communications 53 (1985) 1005–1008.
[13] V.K. Mittal, P. Chandramohan, B. Santanu, M.P. Srinivasan, S. Velmurugan, S.V. Narasimhan, Solid State Communications 137 (2006) 6–10.
[14] B.P. Ladgaonkar, P.N. Vasambekar, A.S. Vaingankar, Journal of Magnetism and Magnetic Materials 210 (2000) 289.
[15] R.D. Waldron, Physical Review 99 (1955) 1727–1735.
[16] S.J. Keny, J. Manjanna, G. Venkateswaran, R. Kameswaran, Corrosion Science 48 (2006) 2780–2798.
[17] In: Dino Fiorani (Ed.), Surface Effects in Magnetic Nanoparticles, first ed., Springer, New York, 2005.
[18] K. Nadeem, H. Krenn, T. Traussnig, R. Würschum, D.V. Szabo, I. Letofsky-Papst, Journal of Applied Physics 111 (2012) 113911.
[19] K. Nadeem, H. Krenn, T. Traussing, I. Letofsky-Papst, Journal of Applied Physics 109 (2011) 013912.
[20] S.A. Morrison, C.L. Cahill, E.E. Carpenter, S. Calvin, R. Swaminathan, M.E. McHenry, V.G. Harris, Journal of Applied Physics 95 (2004) 6392.
[21] A. Goldman, Modern Ferrite Technology, second ed., Springer, New York, 2006.
[22] D. Fiorani, A.M. Testa, F. Lucari, F. D'Orazio, H. Romero, Physica B-Condensed Matter 320 (2002) 122–126.
[23] S. Linderoth, P.V. Hendriksen, F. Bødker, S. Wells, K. Davis, S.W. Charles, S. Mørup, Journal of Applied Physics 75 (1994) 6583.
[24] S. Mørup, Europhysics Letters 28 (1994) 671.
[25] S. Middey, S. Jana, S. Ray, Journal of Applied Physics 108 (2010) 043918.
[26] R.H. Kodama, A.E. Berkowitz, E.J. McNiff, S. Foner, Physical Review Letters 77 (1996) 394.
[27] R.H. Kodama, A.E. Berkowitz, Physical Review B 59 (1999) 6321.